

THE INSTITUTE OF PAPER CHEMISTRY, APPLETON, WISCONSIN

**IPC TECHNICAL PAPER SERIES
NUMBER 130**

**A MATHEMATICAL MODEL OF COMPRESSIVE
STRENGTH IN PAPERBOARD**

C. C. HABEGER AND W. J. WHITSITT

SEPTEMBER, 1982

A MATHEMATICAL MODEL OF COMPRESSIVE STRENGTH IN PAPERBOARD

Charles C. Habeger and William J. Whitsitt

The Institute of Paper Chemistry, Appleton, WI 54912

ABSTRACT

Experimental evidence for a correlation between paperboard edgewise compressive strength and the product of the in-plane normal stiffness and out-of-plane shear stiffness is presented. A mathematical theory, which describes compressive failure as interlaminae shear failure due to prebuckling bending of an initially curved "critical" lamina, is developed. The theory is in accord with failure analysis observations and with the empirical relationship.

LIST OF SYMBOLS

B_1, B_2, D_1, D_2	Constant multipliers in ϕ determination
c	Plate thickness (caliper)
C_2	$-2C_{13} + (C_{11} C_{33} - C_{13}^2)/C_{55}$
C_{ij}	Bulk elastic stiffnesses of the medium
C'_{11}	Planar stiffness of the critical lamina
k	Wave number in the x_1 -direction
ℓ	Exponential coefficient in the x_3 -direction
ℓ_{\pm}	$k[(C_2 \pm (C_2^2 - 4C_{33} C_{11})^{1/2})/2C_{33}]^{1/2}$
L	Span length
RW	Roughness - weakness factor, $\delta A_0 C_{55}/t \tau_f$
t	Critical lamina thickness
T	Distance from the critical lamina to the plate surface
U_m	Elastic energy stored in the medium
U_p	Elastic energy stored in the critical lamina
x_1	Distance along the span
x_2	In-plane distance normal to the span
x_3	Distance along the thickness direction
δA	Incremental change in amplitude
δA_0	Initial curvature amplitude
ϵ	Normal strain in the critical lamina
ϵ_{ij}	Medium strain tensor
λ	Wavelength
σ	Compressive stress
σ_c	Compressive strength
τ_{ij}	Stress tensor
τ_f	Medium shear strength
ϕ	Airy stress potential

BACKGROUND

Compressive strength plays a significant role in determining the mechanical performance of many paperboard products. For example, the single most important structural requirement of the corrugated box is box compressive strength. McKee et al.¹ showed that box compressive strength is primarily dependent on the edgewise compressive strength of the corrugated board and, ultimately, on the edgewise compressive strengths of the component paperboards.

As in the case of most thin sheet materials, there are experimental difficulties in measuring edgewise compressive strength. Buckling of the test specimen must be avoided to determine the intrinsic edgewise compressive strength. Much of the recent work has been concerned with the development of suitable edgewise compressive strength test procedures.²⁻⁵

Under edgewise compressive loads, visual examination of micrographs shows that the sheet expands and the voids enlarge. Fiber bond disruptions along planes of weakness occur as the sheet fails. The planes of voids and weak bonding reflect the layered structure of paper and paperboard, i.e., in normal machine-made papers the fibers lie almost flat, layered on top of each other⁶. Sachs and Kuster⁷ suggest that failure occurs due to a combination of the enlargement of voids, tearing of fiber cell walls, and separation between fiber layers.

Compressive strength increases with sheet density, which depends on the degree of fiber-to-fiber bonding. Seth⁸ and Fellers⁹ indicate that compressive strength may be limited by the compressive strength of the fibers for well-bonded sheets. Work at The Institute of Paper Chemistry shows that compressive strength is affected by the fiber compressive moduli.¹⁰

1. INTRODUCTION

With span length much greater than the thickness, failure under edgewise compression of paperboard is well represented by buckling of an Euler plate. Consider a plate of thickness c gripped by two clamps separated by a distance L . Assume the sample width is infinite and apply a coordinate system with x_1 axis along the span, x_2 axis along the width, and x_3 axis in the thickness direction. If L is much greater than c , the compressive stress necessary to cause buckling can be determined from the Euler approximation. Here the following assumptions are made:¹¹ (1) deflections are small; (2) loads are resisted only by bending moments; (3) the 1-2 plane in the middle of the plate does not change length during bending; (4) sections of the 2-3 plane rotate during bending but remain undistorted and normal to the middle plane; (5) the thickness is much less than the other dimensions; and (6) the material is homogeneous and elastic. With these assumptions, the critical stress, σ , is calculated as a function of C'_{11} , the planar stiffness, and λ , the wavelength at which buckling occurs. The result is

$$\sigma = \frac{\pi^2}{3} \frac{c^2}{\lambda^2} C'_{11} \quad (1)$$

The planar stiffness differs slightly from the bulk stiffness, C_{11} , and from the Young's modulus; it is the ratio of normal stress to normal strain when no strain is allowed normal to the x_2 axis and there is no stress normal to the x_3 axis. From eqn (1), the value of σ_c decreases with λ ; therefore, buckling will first occur at the longest wavelength which complies with the boundary conditions. For a rigidly clamped plate the longest possible wavelength is L , the span. This means that the buckling load as function of span is:

$$\sigma_c = \frac{\pi^2}{3} \frac{c^2}{L^2} C_{11} \quad (2)$$

As L becomes smaller, eqn (2) begins to overestimate σ_c , because there are buckling deformations which do not meet the Euler assumptions and which have lower energies of deformation than the Euler plate. For plates with isotropic elastic properties, significant deviation from eqn (2) occurs when $c/L \lesssim 6$. Paperboard, however, is very anisotropic,¹² the out-of-plane stiffnesses being much smaller than the in-plane values. Because of this, as will be discussed later, the Euler approximation is invalid at $c/L \lesssim 100$.

If the critical compressive load of paperboard is plotted as a function of L/c , the resulting curve can be separated into four regions.² For $L/c \lesssim 100$, Euler's approximation is proper. When $1 \lesssim L/c \lesssim 10$ a plateau region is found in which σ_c is not a function of span. Here the load is limited by the compressive strength of the paperboard and Euler's equation does not apply. The area in between could be called the Euler-plateau transition region. At extremely short spans, critical compressive loads increase above the plateau, and failures are attributed to compressive failure of the fibers.^{2,8,9} Compressive strength is defined as the critical load in the plateau region. This is clearly out of the realm of the Euler Model, and some other explanation is necessary.

Several models of compressive instabilities in homogeneous elastic plates have been developed. Perhaps the best known and most complete is the one presented by Biot.¹³ This provides a description of failures in homogeneous plates with small span to caliper ratios. Unfortunately, much of the development is directed toward incompressible materials, a most inappropriate assumption for paperboard. However, it is possible to approximate the Biot results for compressible plates with out-of-plane stiffnesses much less than in-plane stiffnesses. By doing this, one finds that there is a plateau region in which compressive strength is about 90% of the slide modulus, where the slide modulus¹³ is an incremental shear modulus under

compression and is closely related to C_{55} , the normal shear modulus in the 1-3 plane. This approach has been applied to paperboard by Perkins and McEvoy.¹⁴ Their measured values of C_{55} are much greater than the measured values of compressive strength; however, it is the slide modulus at failure (not the small strain C_{55} which they measured) that is important. This is presumably smaller than the measured C_{55} , and the possibility of good agreement with the Biot picture is preserved.

An investigation of postfailure morphology of paperboard gives insight into mechanisms of compressive failure. Compressive failure involves delamination and buckling of fiber level laminae.⁷ There is a layered structure, existing before compression, that buckles during failure. From failure analysis photomicrographs, such as Fig. 1, it appears that the geometry of the compressive instabilities is governed by the fiber level structure of the sheet. For homogeneous models, the geometry of the instabilities is determined by the elastic properties of the media and the dimensions of the plate. This is not the case here, since fiber level inhomogeneities are of the same order of size as wavelengths encountered in failure of the homogeneous plates. The morphology of the failure is clearly dictated by the fiber level microstructure in the sheet.

[Figure 1 Here]

Another reason for rejecting homogeneous models, such as Biot's, can be taken from an empirical relationship between elastic moduli and compressive strength. Figure 2 demonstrates a linear relationship between σ_c and $C_{11}^{1/2} C_{55}^{1/2}$ for handsheets made from a variety of wood species. Douglas-fir, loblolly pine, and Virginia pine chips were separated into earlywood and latewood fibers, and sheets of different densities were made by varying the wet pressing. In addition, a hardwood species, gum, was pulped and sheets produced at various densities. Notice from Fig. 2 that the data all fall on the same curve in spite of the wide differences in furnish. When σ_c is

plotted versus other physical properties, such as C'_{11} , density, or C_{55} , the plots break down into individual curves for each furnish. The $C'_{11}C_{55}$ parameter unites all the results into a single relationship. Another example of this is given in Fig. 3. Here a series of anisotropic sheets¹⁵ was formed at varying levels of fiber alignment, density, and wet straining. They are all from the same Douglas-fir furnish and have the same basis weight. Again, the compressive strength for this wide range of sheet parameters can be expressed as a function of $C'_{11}C_{55}$. When σ_c is plotted versus other physical properties, a multitude of curves results. Further details on this correlation will be published elsewhere. The Biot Model (as well as the other homogeneous models) is at variance with these empirical results, because compressive strength cannot be determined from C_{55} alone. However, there is a simple relationship between σ_c and elastic properties, and this indicates that the value of the critical load can be predicted from a simple model of failure.

[Figures 2 and 3 here]

A more critical test of this correlation is to plot it in terms of parameters normalized by the density. This is because part of the correlation may be explained by the common density dependence of the compressive strength and stiffness. The data from Fig. 2 and 3 are replotted in terms of strength divided by density and stiffness divided by density in Fig. 4 and 5, respectively. The correlations are not as good, but they are still impressive.

[Figure 4 and 5 here]

The $C'_{11}C_{55}$ term is not the only combination of elastic parameters that correlates well with σ_c . Baum¹⁶ has shown that the in-plane shear modulus, C_{66} , is proportional to $(C'_{11}C'_{22})^{1/2}$ for paper sheets. The proportionality also holds fairly well for out-of-plane shear moduli, e.g., $C_{55} \propto (C'_{11}C_{33})^{1/2}$. This empirical relationship can be used to express $C'_{11}C_{55}$ in terms of other combinations of C'_{11} , C_{55} , and C_{33} and produce other parameters that predict σ_c . The end result is that σ_c depends on

a combination of elastic parameters (usually a combination of an in-plane stiffness and an out-of-plane stiffness).

The above statements are taken to mean that there should be a simple mathematical model of compressive strength in the plateau region. It cannot be a homogeneous model; it must account for the heterogeneity of paperboard. However, since homogeneity assumptions do simplify the calculations, a manageable model must retain as much homogeneity as possible.

2. THEORY

The model described is chosen to have a minimal amount of heterogeneity, while still being consistent with observations from failure analysis. When a failed sheet is sectioned and examined, the sheet appears to have divided itself into platelike "laminae" aligned in the plane of the sheet. In the region of failure the laminae have buckled individually and sheared from the adjacent laminae. Therefore, the idea is to consider the sheet to be a composite of laminae with thicknesses of the order of a fiber thickness. One of these laminae is destined to be the critical lamina, the lamina in which the failure initiates. The model singles out the critical lamina and treats the rest of the sheet as a continuous orthotropic medium. The lamina is thin enough to fail by Euler buckling in the test span; however, buckling of the critical lamina is resisted by the stiffness of the media as well as the stiffness and moment of inertia of the Euler plate. The critical lamina is not necessarily the weakest link, but rather a section that carries a sufficient load so that its failure can lead to total sheet collapse.

Failure by two different mechanisms is analyzed: (a) buckling of an initially flat plate and (b) failure when the maximum shear strength in the medium is exceeded because of buckling deformations near an initially curved lamina. The first mechanism is actually a homogeneous model in disguise. Since one lamina must deform as an

Euler beam, only a subset of the deformations possible in a general homogeneous model is allowed. As expected, the analysis yields a compressive strength greater than that which a homogeneous model would give. The second case is proposed to represent compressive failure of paperboard. It is a truly heterogeneous model, since shear weakness is placed at the boundary of an Euler plate which deforms but does not yield. The plate curvature and medium shear strength can be adjusted to make the predicted σ_c much less than in the homogeneous models. The first case is included, because many of the results from the flat plate analysis are used in the curved plate development.

The major assumptions used in both the flat and curved lamina models are listed below. (1) The critical lamina is an Euler plate. (2) The compressive stress is uniformly distributed. The stress on the critical lamina is equal to the overall compressive stress, σ . (3) The surfaces of the two surrounding media are in rigid contact with the lamina, and deformations inside the media are found from the elastic state equations subject to zero stress boundary conditions at the sheet surface and continuity of deformation at the medium-lamina interface. To first order, the deformations at the surface of the lamina are only in the x_3 -direction. The second order effects due to in-plane deformations in the lamina will be ignored in calculating deformations in the media. (4) The deformations are taken to be independent of the x_2 -direction. In fact, a condition of plane strain in the 1-3 plane is assumed. This complies with the clamping in the actual tester which prevents x_2 -direction deformation at the clamps. The width is large compared with the span, so that Poisson effects at the edges can be neglected. (5) Only the critical lamina is under compression. This is justified by noting that the critical lamina has a much greater disposition for buckling than its neighbors. The effect of compression in the homogeneous medium is small compared with the attempted buckling of

the critical lamina into the medium. This assumption means that the theory is not valid for large L/c , where failure occurs by overall Euler buckling of the entire plate, and the total load must be considered. For small L/c values, the failure is localized, and the model will give a much lower strength than Euler buckling of the whole plate.

Compressive failure of sandwich constructions has been treated mathematically (see for example the work of Norris et al.¹⁷). The calculations required for the critical lamina models are similar to those for a sandwich with thin, stiff outer layers. However, the boundary conditions in the critical lamina models are different from the sandwich, since the thin layer is in the middle. Also, simplifications, due to the large elastic anisotropy in paperboard, are made in the critical lamina models.

a) Initially Flat Critical Lamina

First the critical load necessary to cause buckling of an initially flat plate of thickness t into an orthotropic medium will be calculated. For an isolated flat plate, buckling occurs when the compressive load becomes large enough that the work it does in a virtual displacement is greater than the energy stored in the bending beam for the same displacement. The virtual displacement is taken in the form $\delta u_{x_3} = \delta A \sin kx_1$ and the critical load is found to depend on k . For an isolated plate the critical load decreases monotonically with k , and buckling occurs at the smallest k compatible with the end conditions. In this case the virtual work per unit area must equal the energy stored in the plate and in the medium per unit area. That is, buckling of the plate occurs when

$$\sigma \delta \epsilon = \delta U_p + \delta U_m. \quad (3)$$

Here $\delta \epsilon$ is the incremental strain in the x_1 direction resulting from the $\delta A \sin kx_1$ deformation in a plate whose middle plane cannot stretch. The values of $\sigma \delta \epsilon$ and

δU_p can be taken from any text book analysis of plate bending. They are

$$\sigma t \delta \epsilon = \sigma t (\delta A)^2 k^2 / 4 \quad (4)$$

and
$$\delta U_p = C_{11}' (\delta A)^2 k^4 t^3 / 48. \quad (5)$$

Now, all that is needed is δU_m , i.e., the incremental energy of deformation per unit area in the media on both sides of the critical lamina. This can be taken from the following calculation of the energy per unit area in an orthotropic plate of thickness T with $\delta u_{x_3} = \delta A \sin kx_1$ and $\delta u_{x_1} = 0$ on one surface and $\tau_{33} = \tau_{31} = 0$ on the other surface.

Since plane strain is assumed ($\epsilon_{21} = \epsilon_{22} = \epsilon_{23} = 0$), the stress-strain relationships for the elastic, orthotropic media are

$$\tau_{11} = C_{11} \epsilon_{11} + C_{13} \epsilon_{33}, \quad (6)$$

$$\tau_{33} = C_{13} \epsilon_{11} + C_{33} \epsilon_{33}, \text{ and} \quad (7)$$

$$\tau_{13} = 2 C_{55} \epsilon_{13}. \quad (8)$$

The equations of static equilibrium are

$$\tau_{11,1} + \tau_{13,3} = 0 \quad (9)$$

and
$$\tau_{33,3} + \tau_{13,1} = 0. \quad (10)$$

Equations (9) and (10) are satisfied identically if the τ_{ij} 's are taken from an Airy stress potential¹⁸ ϕ ; that is, if $\tau_{11} \equiv \phi_{,33}$, $\tau_{33} \equiv \phi_{,11}$, and $\tau_{13} \equiv -\phi_{,13}$, then eqns (1) and (2) are automatically fulfilled.

In addition to the equations for elastic equilibrium, the compatibility equations must be obeyed. For the plane strain case, compatibility is fulfilled if

$$\epsilon_{11,33} + \epsilon_{33,11} = 2 \epsilon_{13,13}. \quad (11)$$

Expressing ϵ_{ij} in terms of ϕ , eqns (11) becomes

$$C_{11} \phi_{,1111} + \left[\left(\frac{C_{11}C_{33} - C_{13}^2}{C_{55}} \right) - 2C_{13} \right] \phi_{,1133} + C_{33} \phi_{,3333} = 0. \quad (12)$$

So, any ϕ obeying eqn (12) gives an admissible solution to the plane strain elastic equilibrium equations.

Assuming a solution of the form $\phi = f(x_3) \sin kx_1$ and inserting into eqn (12) imposes the following restriction on $f(x_3)$.

$$C_{11} k^4 f(x_3) - C_2 k^2 f(x_3)'' + C_{33} f(x_3)'''' = 0, \quad (13)$$

Where $C_2 = -2C_{13} + (C_{11}C_{33} - C_{13}^2)/C_{55}$. A solution of the form $f(x_3) = e^{\ell x_3}$ is satisfactory if

$$\ell = \pm k \left[\frac{C_2 \pm (C_2^2 - 4C_{33}C_{11})^{1/2}}{2C_{33}} \right]^{1/2} = \pm \ell_{\pm} \quad (14)$$

Thus an acceptable form for ϕ with four arbitrary constants, B_1, B_2, D_1 and D_2 is

$$\phi = [B_1 \sinh \ell_+ x_3 + B_2 \sinh \ell_- x_3 + D_1 \cosh \ell_+ x_3 + D_2 \cosh \ell_- x_3] \sin kx_1. \quad (15)$$

The values of $B_1, B_2, D_1,$ and D_2 can be chosen so that the four boundary conditions are met. This is done when the following linear simultaneous equations are fulfilled.

$$\begin{bmatrix} \sinh \ell_+ T & \sinh \ell_- T & \cosh \ell_+ T & \cosh \ell_- T \\ t \ell_+ \cosh \ell_+ T & t \ell_- \cosh \ell_- T & t \ell_+ \sinh \ell_+ T & t \ell_- \sinh \ell_- T \\ 0 & 0 & \frac{(C_{13}k^2 + C_{33}\ell_+^2)t^2}{C_{11}} & \frac{(C_{13}k^2 + C_{33}\ell_-^2)t^2}{C_{11}} \\ \frac{(C_{13}\ell_+^2 + C_{11}k^2)tC_{11}}{\ell_+(C_{11}C_{33} - C_{13}^2)} & \frac{(C_{13}\ell_-^2 + C_{11}k^2)tC_{11}}{\ell_-(C_{11}C_{33} - C_{13}^2)} & 0 & 0 \end{bmatrix} \begin{bmatrix} \frac{B_1}{C_{11} \delta A t} \\ \frac{B_2}{C_{11} \delta A t} \\ \frac{D_1}{C_{11} \delta A t} \\ \frac{D_2}{C_{11} \delta A t} \end{bmatrix} = \begin{bmatrix} 0 \\ 0 \\ 0 \\ -1 \end{bmatrix} \quad (16)$$

Paperboard is extremely anisotropic, the z-direction stiffness being much smaller than the in-plane stiffnesses. Also, failure often occurs at a wavelength less than T ; therefore, approximate solutions to eqn (16) when $C_{11} \gg C_{33}$, $C_{11} \gg C_{13}$, $C_{11} \gg C_{55}$, and $e^{kT} \gg 1$ will be of interest later. A straightforward calculation shows that in these limits the coefficients are

$$B_1 \approx -D_1 \approx \frac{(C_{13} + C_{55})C_{55}^{3/2} \delta A}{kC_{11}C_{33}^{1/2}}, \text{ and} \quad (17)$$

$$B_2 \approx -D_2 \approx \frac{-C_{55}^{1/2}C_{33}^{1/2} \delta A}{k} \quad (18)$$

Now δU_m can be calculated for the general case and also in the limit of high anisotropy and deep embedment. The stored energy, δU_m , is equal to the work done by forces acting on the boundary of the medium necessary to cause a δA deformation. So

$$\delta U_m = \frac{-k}{2\pi} \int_0^{2\pi/k} \left[\frac{\tau_{33} \delta u_{x3}}{2} \right]_{z=0} dx_1. \quad (19)$$

Using $\tau_{33} = -k^2 \phi$, $[\phi]_{z=0} = (D_1 + D_2) \sin kx_1$, and $[\delta u_{x3}]_{z=0} = \delta A \sin kx_1$, the integration gives

$$\delta U_m = k^2 \delta A (D_1 + D_2) / 4. \quad (20)$$

For the limiting case the expressions in eqns (17) and (18) reduce this to

$$\delta U_m \approx C_{33}^{1/2} C_{55}^{1/2} k (\delta A)^2 / 4. \quad (21)$$

Inserting the results of eqns (20) into eqn (3) produces the following expression for σ as a function of k .

$$\sigma = \frac{C_{11}' k^2 t^2}{12} + \frac{(D_1 + D_2)_1}{t \delta A} + \frac{(D_1 + D_2)_2}{t \delta A} \quad (22)$$

The expressions $(D_1+D_2)_1$ and $(D_1+D_2)_2$ are found by solving eqn (16) with T equal to the distance from the critical lamina to the top and bottom surfaces, respectively. This can be done numerically and σ can be plotted versus λ . The results depend on t/c and to some extent on the location of the critical lamina to the surface. When the critical lamina is near the surface, σ is less than for interior laminae. Figure 6 presents plots of σ/C_{11}' versus λ/t for different values of c , critical lamina locations, and stiffness ratios. Curve 1 is a single lamina with no reinforcing medium. It is simply the Euler curve for an isolated lamina. Curve 2 is for a plate two laminae thick. At larger wavelengths it is stronger than the single Euler plate; however, σ still decreases monotonically with λ . As c/t increases, a minimum occurs in the σ versus λ curve. Curve 3 is the lowest value of c/t at which this happens. Here the critical lamina is on the surface and the sheet is four laminae thick. As the sheet becomes thicker, the location of the minimum approaches a limit. In fact, once the plate is about eight laminae thick these values are quite stable with changing c/t . Curves 4 and 5 are respectively eight- and sixteen-laminae-thick sheets, the critical lamina being one of the two center ones. Curves 1 through 5 are all for media with elastic anisotropy typical of paper.¹² Curve 6 is a center lamina of a 16-laminae-thick isotropic plate. It is presented as a contrast to the paper case where there is large elastic anisotropy.

[Figure 6 here]

The expression for σ is simplified in the limiting case where eqn (22) is valid.

Here

$$\sigma \approx \frac{C_{11}' t^2 k^2}{12} + \binom{2}{1} \frac{C_{33}^{1/2} C_{55}^{1/2}}{kt} \quad (23)$$

In the above equation the 2 is for a center lamina and the 1 is for a surface lamina; other lamina locations have intermediate values. The value of λ for the minimum buckling load, σ_c , can be found by setting $d\sigma/dk$ to zero. The result is

$$k_{opt} \approx \left[\frac{\binom{2}{1} 6C_{33}^{1/2} C_{55}^{1/2}}{C'_{11}} \right]^{1/3} \frac{1}{t} \quad (24)$$

When this is inserted into eqn (23), an approximate value for σ_c is obtained.

$$\sigma_c \approx \binom{1.31}{0.83} [C'_{11} C_{33} C_{55}]^{1/3} \quad (25)$$

The location of the minima in the numerically generated curves, such as those in Fig. 6, can be compared with the asymptotic values in eqns (24) and (25). For plates with anisotropy typical of paper the locations of the minima determined by the two methods differ by less than 5% when the plate is 7 laminae thick or more. The cross symbols on Fig. 4 mark the location of the asymptotic minima for curves 3-6.

The value of σ_c from this curve is more than three times greater than C_{55} ($\approx 0.018 C'_{11}$), the order of values predicted by the homogeneous theories. This is to be expected, since as yet no real inhomogeneity has been injected into the model. The generality of the deformation has merely been limited and compression over much of the plate has been ignored.

b) Initially Curved Critical Lamina

Now the case of an initially curved critical lamina bending into a reinforcing orthotropic medium will be studied. In paperboard there is a zone of weakness between the laminae, and shear failure can occur due to prebuckling deformations. The model will not allow buckling of the critical laminae, but when the maximum shear stress in the medium exceeds a limit, the plate yields. A curved plate under compression bends before buckling. The initial curvature can be expressed as a Fourier summation of sinusoidal functions. The Fourier components with wavelengths

near the critical wavelength lead to large deformations of the lamina. It is curvature near this wavelength that results in the prebuckling, shear failure of the medium.

First the deformation of a plate with initial curvature, $\delta A_0 \sin kx_1$, will be found as a function of σ and k . The analysis is similar to the first case, except the work done by σ depends on δA_0 and a nonzero deformation equilibrium can be lamina or in the medium. When σ is applied, the deformation, $U_z = (\delta A + \delta A_0) \sin kx_1$, is found by requiring the total energy to be a minimum.

$$\sigma t \delta \epsilon = \delta U_p + \delta U_m \quad (26)$$

Now the virtual work term becomes

$$\sigma t \delta \epsilon = \sigma t (\delta A + \delta A_0) \delta A k^2 / 2, \quad (27)$$

while the other terms are unchanged. Therefore, the equilibrium condition is

$$\frac{\sigma t k^2 (\delta A + \delta A_0)}{2} = \frac{C_{11}' \delta A k^4 t^3}{24} + k^2 \delta A \left[\frac{(D_1 + D_2)_1 + (D_1 + D_2)_2}{\delta A} \right] \quad (28)$$

Solving for the incremental deformation, δA , yields

$$\delta A = \sigma \delta A_0 / \left[\frac{C_{11}' k^2 t^2}{12} + \left[\frac{(D_1 + D_2)_1 + (D_1 + D_2)_2}{t} \right] - \sigma \right] \quad (29)$$

This gives a nonlinear relationship between δA and σ , even though the entire process could be elastic. Now the maximum shear stress in the medium can be calculated.

$$\tau_{13} = -\Phi_{,13} = -k \cos kx_1 [B_1 l_+ \cosh l_+ x_3 + B_2 l_- \cosh l_- x_3 + D_1 l_+ \sinh l_+ x_3 + D_2 l_- \sinh l_- x_3] \quad (30)$$

The maximum stress occurs when $\cos kx = 1$ and $z = 0$; therefore,

$$(\tau_{13})_{\max} = -k \frac{[B_1 \ell_+ + B_2 \ell_-]_L}{C_{11} \delta A t} C_{11} \delta A t . \quad (31)$$

In eqn (31), $[B_1 \ell_+ + B_2 \ell_-]_L$ is taken as the largest value calculated for two media attached to the critical lamina. The maximum shear stress expressed as a function of σ is

$$(\tau_{13})_{\max} = \frac{\sigma \delta A_0 k \left[\frac{[B_1 \ell_+ + B_2 \ell_-]_L}{C_{11} \delta A t} \right]}{\left[\frac{C'_{11} k^2 t^2}{C_{11}^2} + \frac{[(D_1 + D_2)_1 + (D_1 + D_2)_2]}{C_{11} \delta A t} - \frac{\sigma}{C_{11} t} \right]} \quad (32)$$

When $(\tau_{13})_{\max}$ equals the shear strength at the interface, τ_f , failure occurs.

Equation (32) is now solved for σ_c as a function of τ_f .

$$\sigma_c / C_{11} = \frac{\left[\frac{C'_{11} k^2 t^2}{C_{11}^2} + \frac{[(D_1 + D_2)_1 + (D_1 + D_2)_2]}{t \delta A C_{11}} \right]}{\left[1 - \frac{C_{11}}{C_{55}} RW kt \frac{[B_1 \ell_- t + B_2 \ell_+ t]_L}{t \delta A C_{11}} \right]} \quad (33)$$

The term RW symbolizes the "roughness-weakness" factor, $\frac{\delta A_0}{t} \frac{C_{55}}{\tau_f}$. This is the ratio of initial curvature near the critical wavelength to the lamina thickness, a "roughness" factor, multiplied by the ratio of shear modulus to strength, a "weakness" factor.

Equation (16) will give the D and B coefficients in terms of elastic constants, and then σ_c / C_{11} can be plotted vs. λ / t for a given set of elastic constants, plate and lamina dimensions, and value of RW. Figure 7 presents some such plots for elastic coefficients typical of paper. The curves are for a plate 20 laminae thick at four different RW values. The critical lamina is taken in the sheet center. The RW = 0 curve is the same as the flat plate buckling condition discussed earlier.

Notice that as the RW factor increases, σ_c (the minimum in critical load) decreases. Realistic values of σ_c well below C_{55} are realized with reasonable values of RW. The value of C_{55}/τ_f of around $100^{19,20}$ and the total Fourier component of amplitudes in the region of the minimum of about $0.01t$ to $1.0t$ seems probable. The straight line in Fig. 7 is the Euler curve for a plate 20 laminae thick. The model curves are expected to be valid only in wavelength regimes where the Euler curve is much higher than the model curves. Notice that the wavelength of the minimum failure stabilizes at about $10t$ for values of RW greater than about 10. Again, these curves are not much of a function of thickness, c , once c is greater than about $7t$. Also, as in the first case, the critical load is less when the critical lamina is on the surface than when it is about $3t$ or more deeper into the plate. Figure 8 is a similar set of curves for a hypothetical isotropic plate. Notice that minimum are not achieved for λ/t greater than 2. Since the assumption of Euler buckling of the lamina is invalid if $\lambda/t < 6$, this model is appropriate for paperboard only, because it is highly anisotropic.

[Figures 7 and 8 here]

As in the flat plate, simplification can be made when $C_{11} \gg C_{55}$, $C_{11} \gg C_{33}$, $C_{11} \gg C_{13}$, and $e^{kT} \gg 1$. In this case eqn (32) becomes

$$(\tau_{13})_{\max} \approx \frac{\sigma_k C_{55} \delta A_o \left[1 - \frac{C_{13} + C_{55}}{(C_{11} C_{33})^{1/2}} \right]}{\left[\frac{C_{11} k^2 t^2}{12} + \binom{2}{1} \frac{C_{55}^{1/2} C_{33}^{1/2}}{kt} - \sigma \right]} \quad (34)$$

In eqn (34) the 2 is for a center lamina and the 1 is for a surface lamina. Taking the derivative of eqn (34) with respect to k and assuming that $(C_{55} C_{33})^{1/2} \gg \sigma_c (kt)_{\text{opt}}$ gives the following approximate values of $(kt)_{\text{opt}}$, the value of kt with the minimum compressive failure load.

$$(kt)_{\text{opt}} \approx \left[\binom{2}{1} 24 \frac{C_{55}^{1/2} C_{33}^{1/2}}{C_{11}} \right]^{1/3} \quad (35)$$

This value of kt is inserted into eqn (34) to give an approximate σ_c .

$$\sigma_c \approx \frac{\begin{pmatrix} 0.454 \\ 0.360 \end{pmatrix} C_{11}^{2/3} C_{55}^{1/6} C_{33}^{1/6}}{RW \left[1 - \frac{C_{13} + C_{55}}{C_{11}^{1/2} C_{33}^{1/2}} \right]}$$

To get eqn (36), it was also assumed that $\sigma_c \ll (C_{11}C_{33}C_{55})^{1/3}$. The location of the minima as predicted by eqns (35) and (36) is marked by a cross for the nonzero RW curves in Fig. 7. Notice that the approximation becomes quite good for large RW values. The cross near the $RW = 0$ curve comes from eqns (24) and (25).

3. DISCUSSION

The results of the curved lamina model are consistent with many of the known characteristics of compressive failure in paperboard. First, a four region critical stress versus L/c curve is predicted with break points in the right regions. See Fig. 9. These plots are made from curves such as those in Fig. 7, after it is assumed that failure under compression will occur at the available wavelength having the least strength. The plate has rigidly clamped edges; therefore, the plate can fail with instabilities at any wavelength less than the span. Failure will occur at the wavelength below span length that has the least strength. For large spans the Euler curve is far below the model curve, and the critical stress vs. L/c curve is the Euler curve of the total plate. As λ decreases, a region is reached where the Euler curve is of the same order of magnitude as the minimum of the model curve. Here neither picture is appropriate; some combination of the two processes is at work. This is the Euler plateau transition region. At lower λ values the Euler curve is much greater than the model curve minimum. In this region the critical stress is σ_c , and the failure wavelength corresponds to that at the minimum of the model curve. At spans less than the wavelength of σ_c , the critical stress again begins to increase. The model becomes invalid as L approach t , and some other process, such as compressive failure of the fiber, dominates. Figure 9 is a set of curves plotted in this way. Each has $RW = 10$ and anisotropy typical of paper. There are curves

the plateau region increases with c/t . The height of the plateau stabilizes for $c/t \geq 6$, and the only effect of increasing c is to extend the plateau to lower L/c values. Increasing the values of RW would lower the plateau and move the transition region to larger L/c values.

[Figure 9 here]

Equation (36) is an approximate relation of the plateau region compressive strength to the elastic moduli and the RW factor. The term $(1 - \frac{C_{13} + C_{55}}{C_{11}^{1/2}C_{33}^{1/2}})$ is not very sensitive to elastic property changes caused by process variable operations. This is because increases in $C_{13}+C_{55}$ are generally accompanied by greater increases in C_{33} . If this part of the function is taken as a constant, a very simple expression for σ_c is found:

$$\sigma_c \propto \frac{C_{11}'^{2/3}C_{55}'^{1/6}C_{33}'^{1/6}}{RW} \quad (37)$$

The RW factor depends on C_{55}/τ_f , but certainly there is a strong correlation between C_{55} and τ_f and their ratio should not vary much as process variables change. At any rate, if RW is assumed to be constant for a given set of process changes and the empirical correlation, $C_{55} \propto C_{33}'^{1/2}C_{11}'^{1/2}$, is used, eqn (37) can be transformed to the empirical relation discussed earlier, $\sigma_c \propto C_{11}'^{1/2}C_{55}'^{1/2}$.

Equation (37) is similar to the earlier discovered empirical relationship, $\sigma_c \propto C_{11}'^{1/2}C_{55}'^{1/2}$, in that σ_c depends on a combination of elastic parameters. To test eqn (37), σ_c is plotted versus $C_{11}'^{2/3}C_{55}'^{1/6}C_{33}'^{1/6}$ for the same samples as in Fig. 2 and 3. These results are presented in Fig. 10 and 11, respectively. Notice that for both Fig. 10 and 11 the data fall near a straight line with a slope of one. Figure 11 shows a good correlation as does Fig. 3; however, Fig. 2 is better than Fig. 10. All of the data for the oriented sheets with constant furnish (Fig. 11) form a single line, while the variable furnish sheets (Fig. 10) seem to divide into

separate lines. This is rationalized by noting that RW may not change with wet straining, wet pressing or fiber orientation, but it could depend on furnish. A major advantage of eqn (37) over the empirical correlation is that the composite curves of Fig. 10 and 11 are quite close to each other, whereas the curves in Fig. 2 and 3 are at different levels.

[Figures 10 and 11 here]

Equation (35) provides an approximate relationship between elastic constants and the ratio of the wavelength of the compressive failure to lamina thickness. This approximate value is within a few percent of the exact solution for a material with paperlike anisotropy and an RW factor greater than 10. For paper anisotropy it predicts that this ratio is of the order of ten. Observations of micrographs, such as Fig. 1, verify that this prediction is in the correct region.

The load-deformation curve for a sample in a compression strength tester becomes nonlinear well below the loads at which yielding occurs in tension. If the compression load is released before failure, some authors have described the sheet as returning to its original shape with little evidence of plastic yields.⁷ This observation is consistent with the picture of elastic bending of a curved lamina into a restraining medium. Equation (29) could be used to calculate the change in amplitude, δA , of a sinusoidal curvature. This could be inserted into eqn (27) to give the x_1 -direction strain as a function of compressive stress. Notice that the stress-strain relationship could be nonlinear, even though linear elastic processes are controlling the action. This is simply because bending of a curved plate gives a nonlinear stress-strain relationship.

The model predicts that σ_c decreases as initial plate curvature increases, if the elastic coefficients do not change. This should not be interpreted to mean that additional lamina curvature necessarily weakens the sheet. This is because

increases in curvature result in greater x_3 -direction alignment of the fibers, which in turn results in greater out-of-plane stiffness. This increase in stiffness could well overpower the increase in RW.

4. BIBLIOGRAPHY

1. R. C. McKEE, J. W. GANDER and J. R. WACHUTA, Paperboard Packaging 48 (8) (Aug., 1963).
2. S. CAVLIN and C. FELLERS, Svensk Papperstid. (9) (1975) pp. 319-32.
3. C. A. JACKSON, J. W. KONING, Jr. and W. A. GUTZ, Pulp Paper Canada 77 (19) (Oct., 1976) pp. T180-3.
4. V. E. STOCKMAN, Tappi 57 (7) (July, 1976) pp. 93-7.
5. R. S. SETH and R. M. SOSZYNSKI, Tappi 62 (10) (Oct., 1979) pp. 125-7.
6. B. RADVAN, C. DODSON and C. G. SKOLD, In Consolidation of the Paper Web, Vol. 1 Transactions of the Symposium at Cambridge, England, 1965.
7. I. B. SACHS and T. A. KUSTER, Tappi 63 (10) (Oct., 1980) pp. 69-73.
8. R. S. SETH, R. M. SOSZYNSKI and D. H. PAGE, Tappi 62 (12) (Dec., 1979) pp. 97-9.
9. C. FELLERS; A. deRUVO and M. HTUN, Tappi 63 (6) (June, 1980) pp. 109-12.
10. To be published.
11. P. S. BULSON, "The Stability of Flat Plates," American Elsevier Publ. Co., N.Y. (1969).
12. R. W. MANN, G. A. BAUM and C. C. HABEGER, Tappi 63 (11) (Feb., 1980) p. 163.
C. C. HABEGER, R. W. MANN and G. A. BAUM, Ultrasonics 17 (1979) p. 57.
13. M. A. BIOT, "Mechanics of Incremental Deformations," John Wiley & Sons, N.Y. (1965).
14. R. W. PERKINS and R. P. McEVOY, Tappi 64 (1981) p. 99.
15. E. H. FLEISCHMAN, Doctoral Dissertation, Appleton, WI, The Institute of Paper Chemistry, 1981.
16. G. A. BAUM, D. C. BRENNAN and C. C. HABEGER, Tappi 64 (8) (Aug., 1981) p. 97.
17. C. B. NORRIS, S. E. WILHELM, H. W. MARCH, C. B. SMITH, and K. H. BOCCER, "Wrinkling of the Facings of Sandwich Construction Subjected to Edgewise Compression" Report 1810, Forest Products Laboratory, Madison, WI (1949).

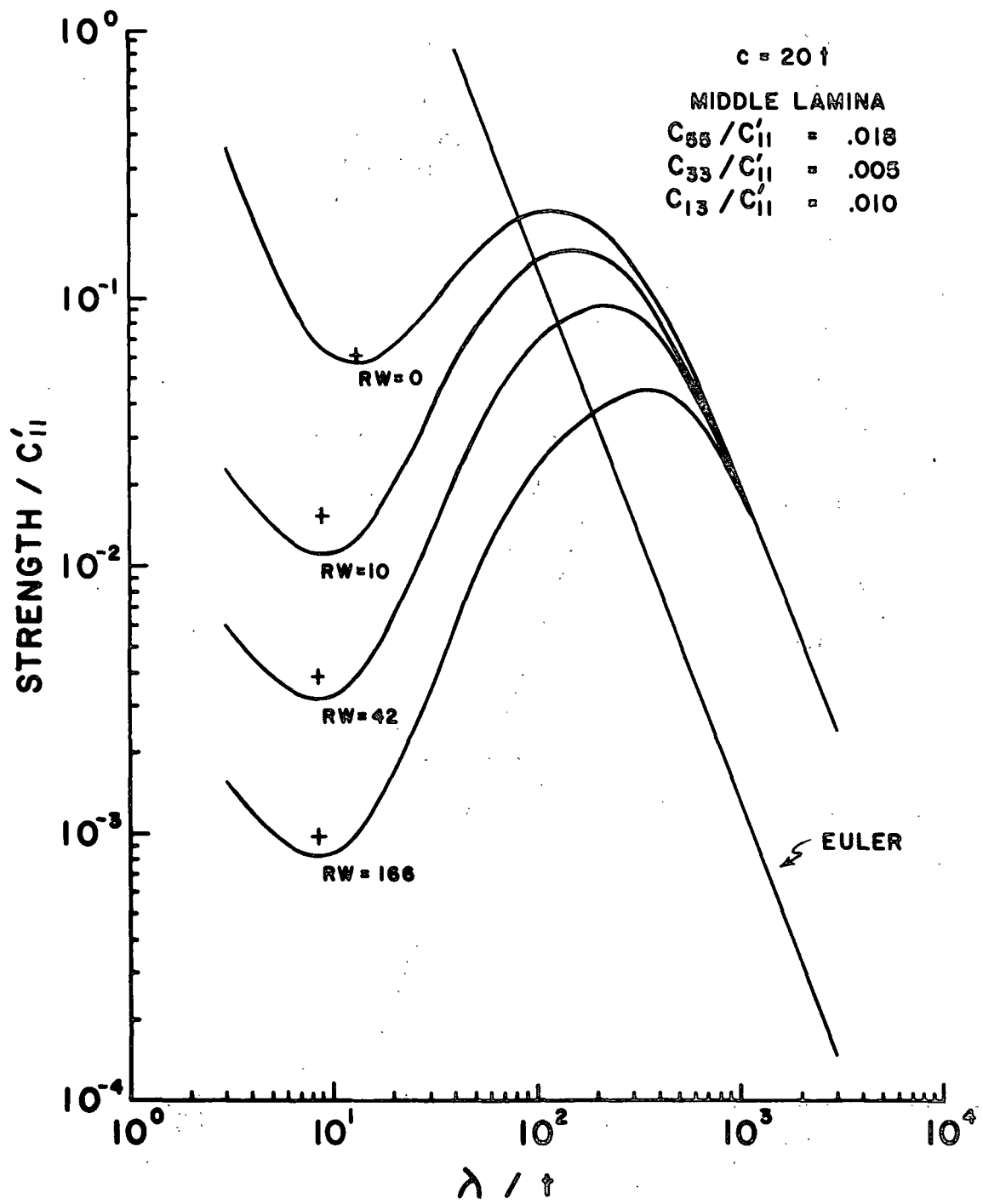


Fig. 7. Plots of strength versus wavelength for middle critical laminae in a sheet 20 laminae thick at varying roughness-weakness factors in anisotropic sheets.

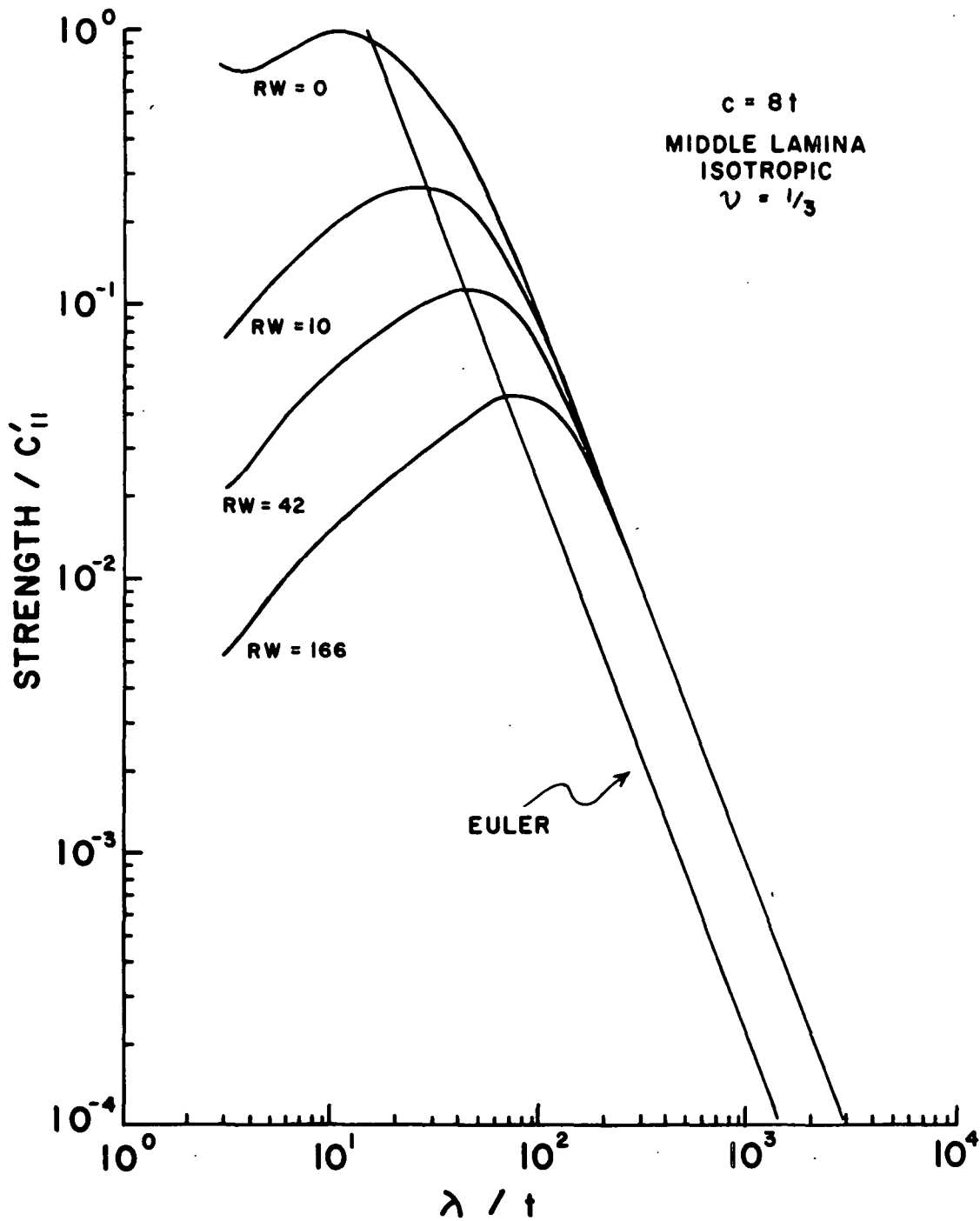


Fig. 8. Plots of strength versus wavelength for middle critical laminae in a sheet 8 laminae thick at varying roughness-weakness factors in isotropic sheets.

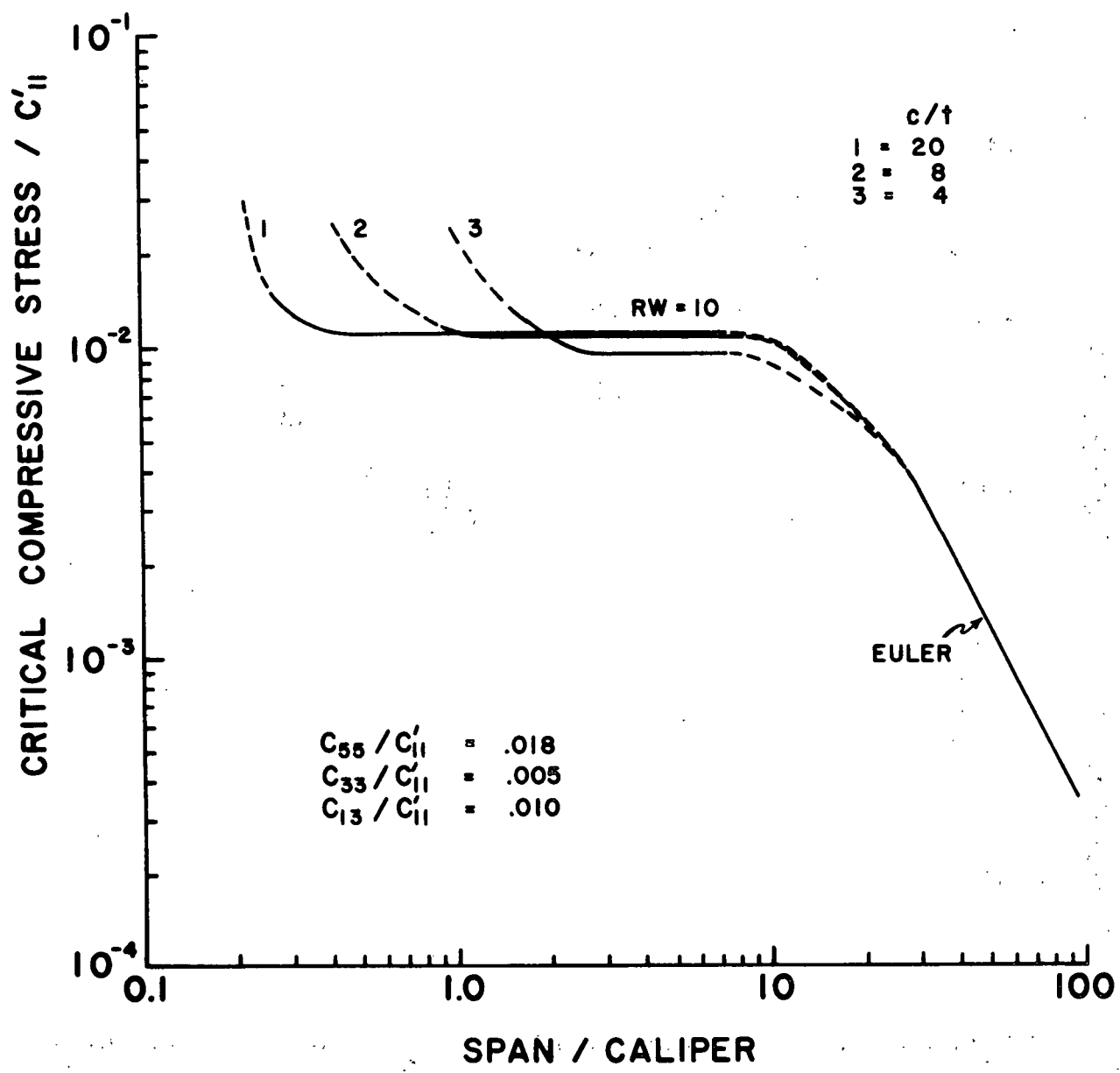


Fig. 9. Plots of critical compressive stress versus span for anisotropic sheets of varying thickness.

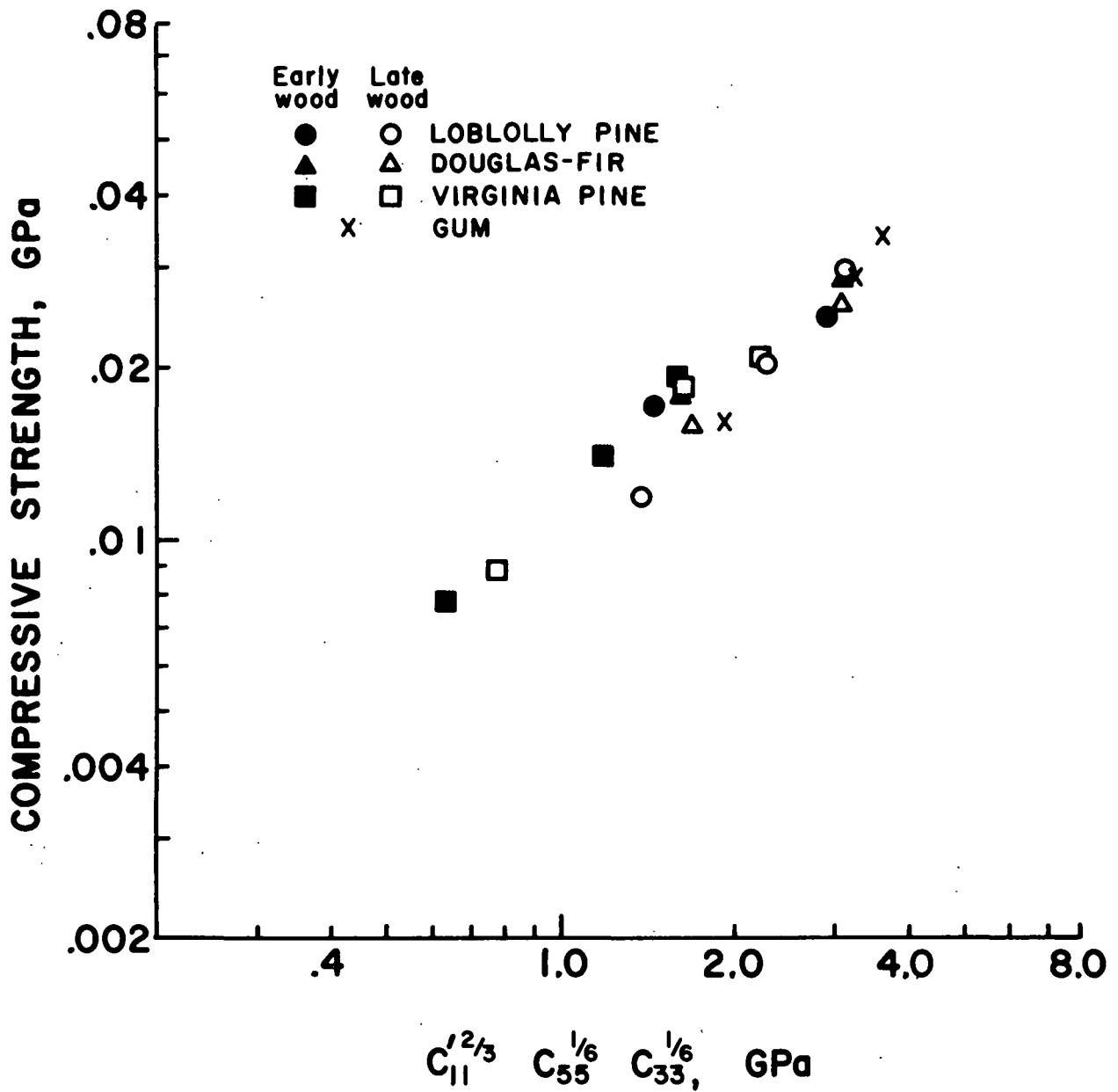


Fig. 10. Relationship between compressive strength and elastic parameters for handsheets.

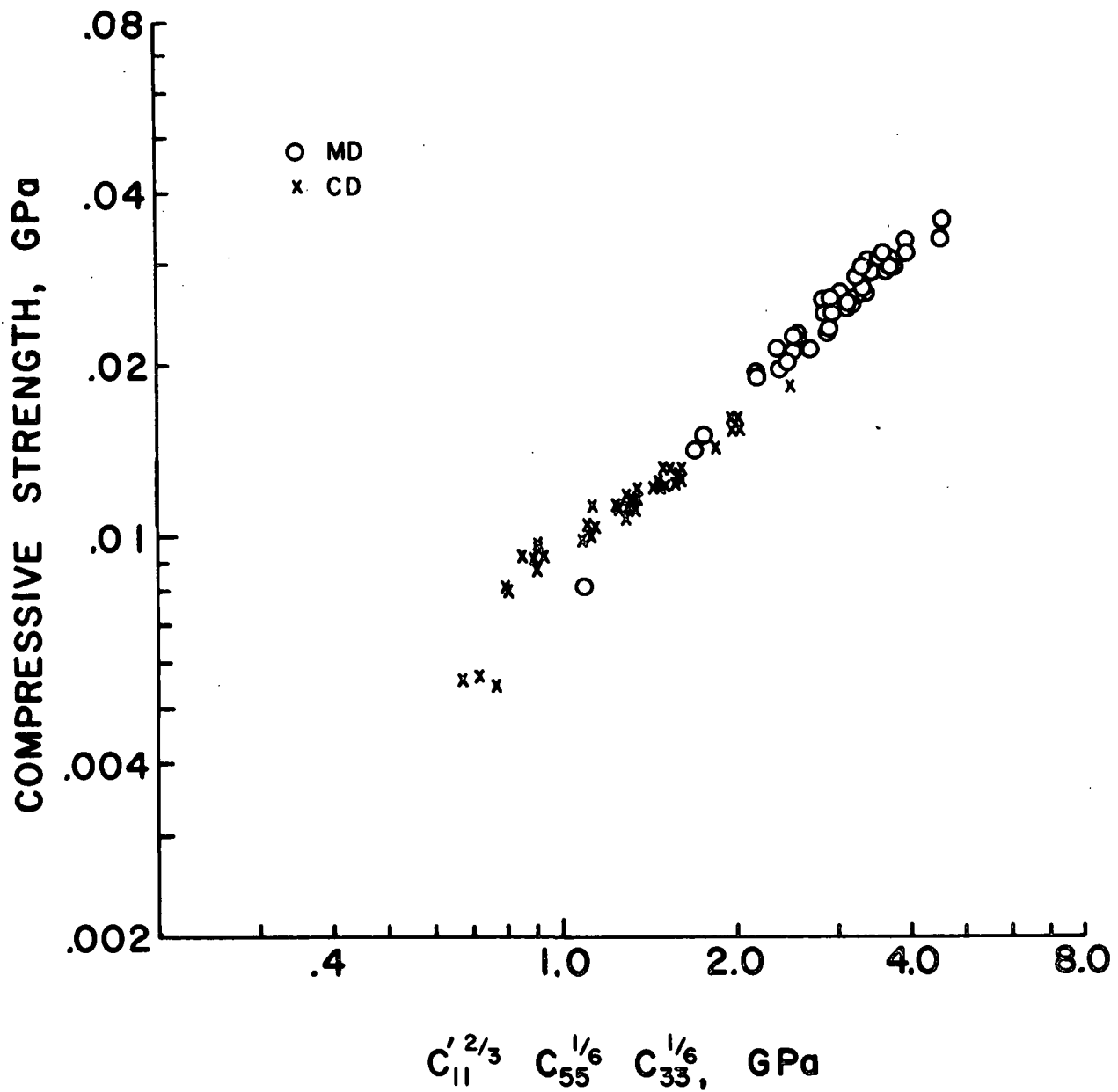


Fig. 11. Relationship between compressive strength and elastic parameters for anisotropic sheets.

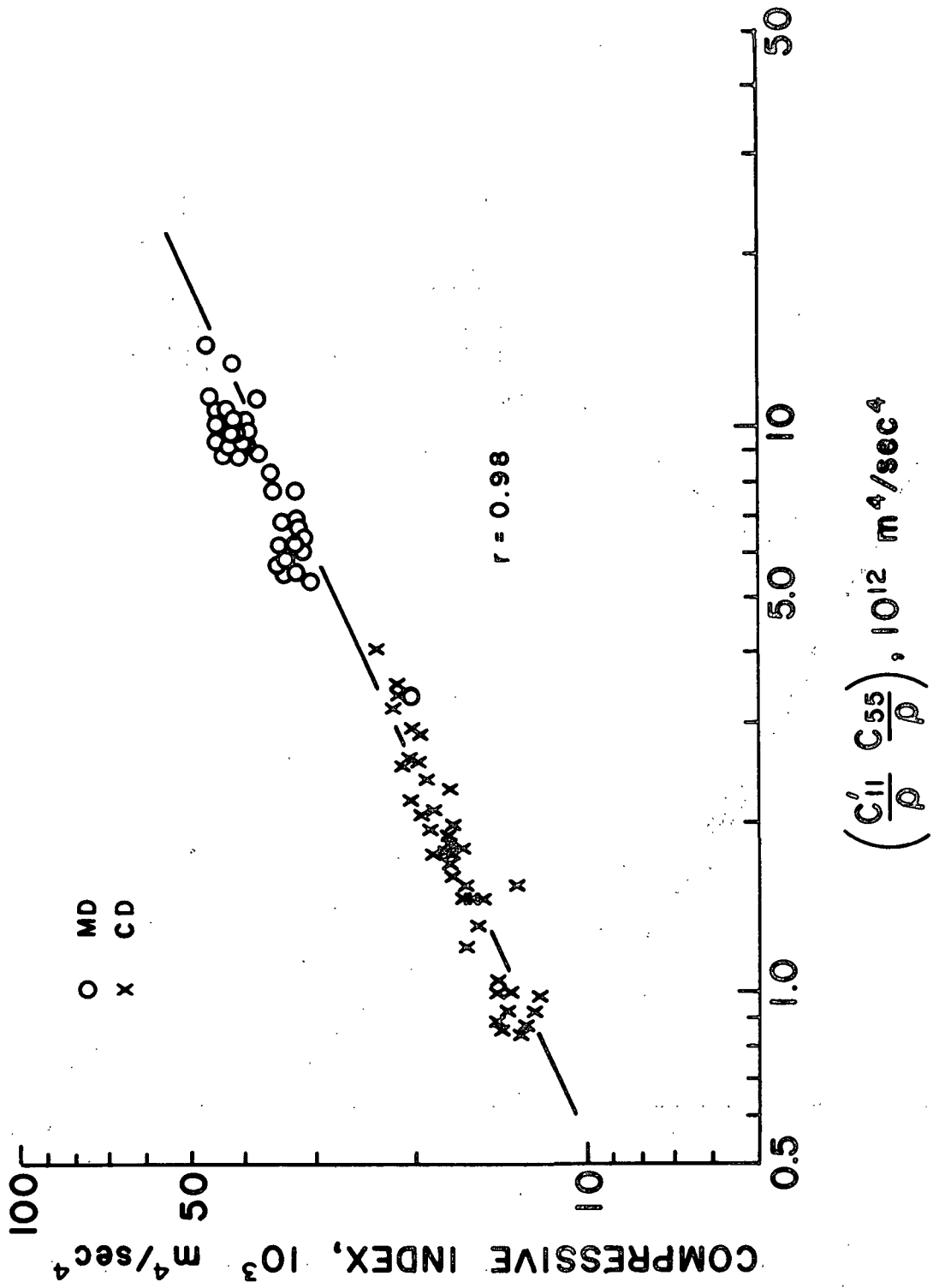


Fig. 5. The data in Fig. 3 plotted in terms of mass intensive parameters.

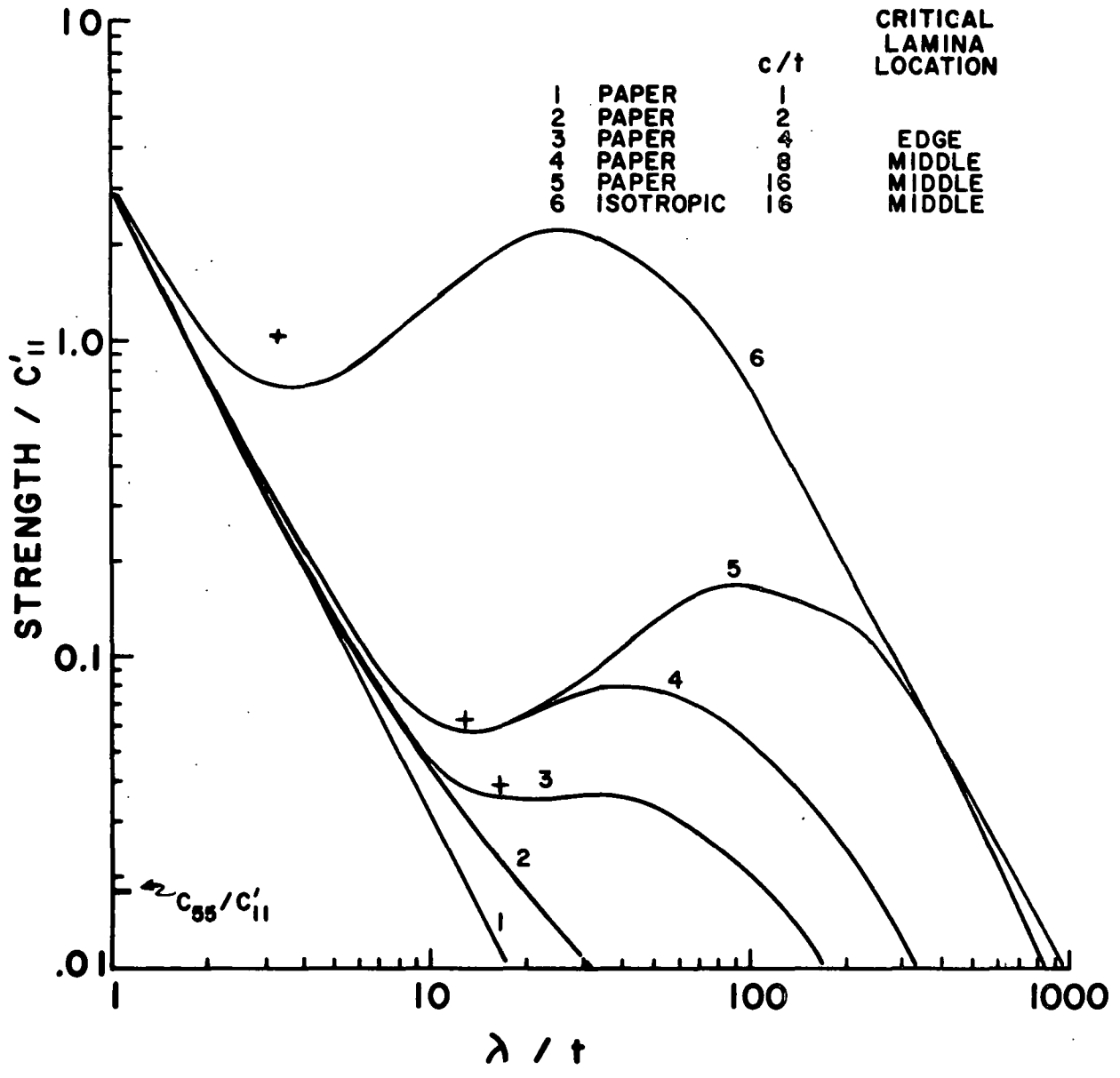


Fig. 6. Plots of strength versus wavelength of failure for critical laminae at varying sheet locations and varying sheet thicknesses.

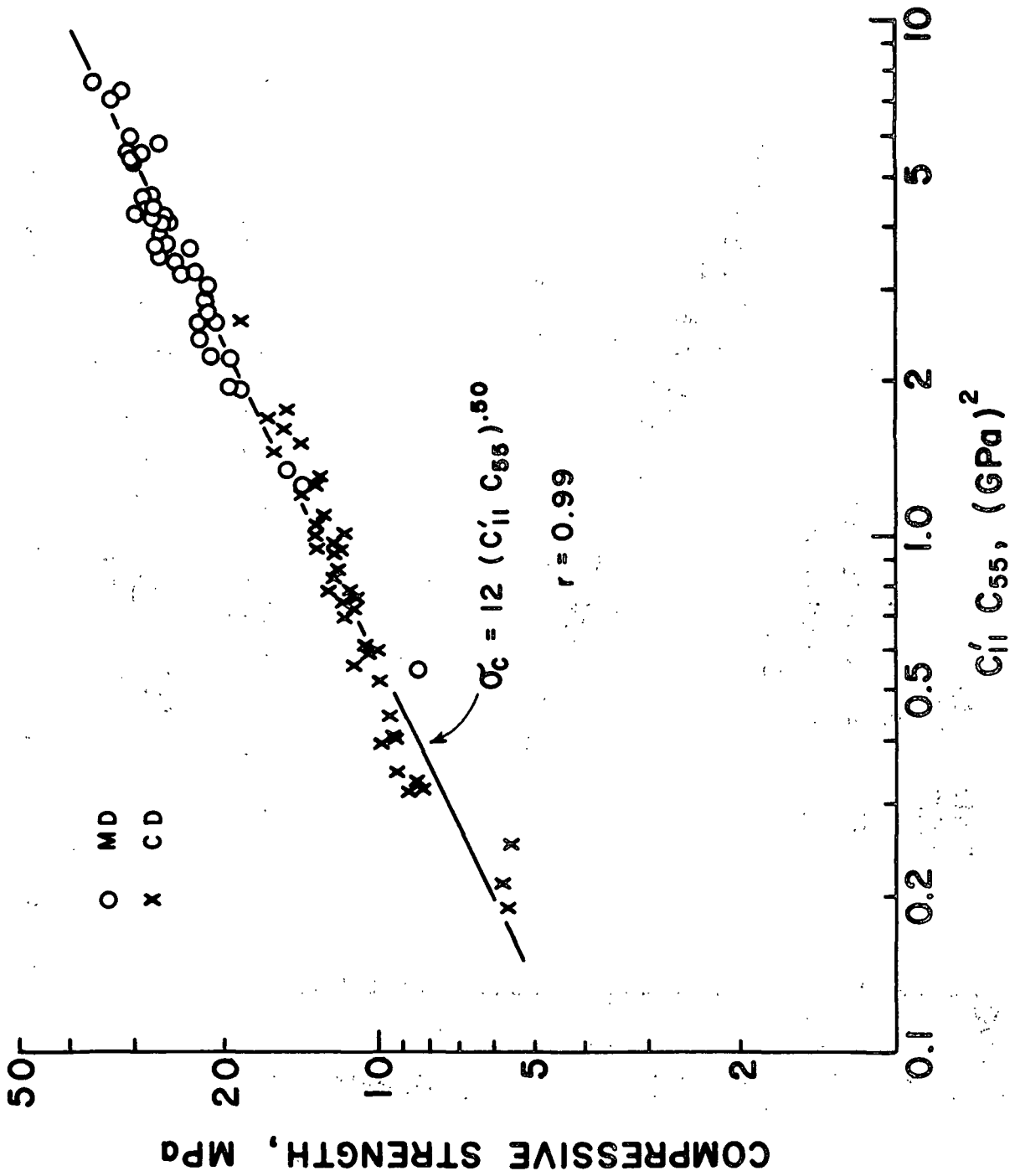


Fig. 3. Empirical relationship between compressive strength and in-plane stiffness times out-of-plane shear stiffness for anisotropic sheets with varying density, fiber orientation, and wet straining levels.

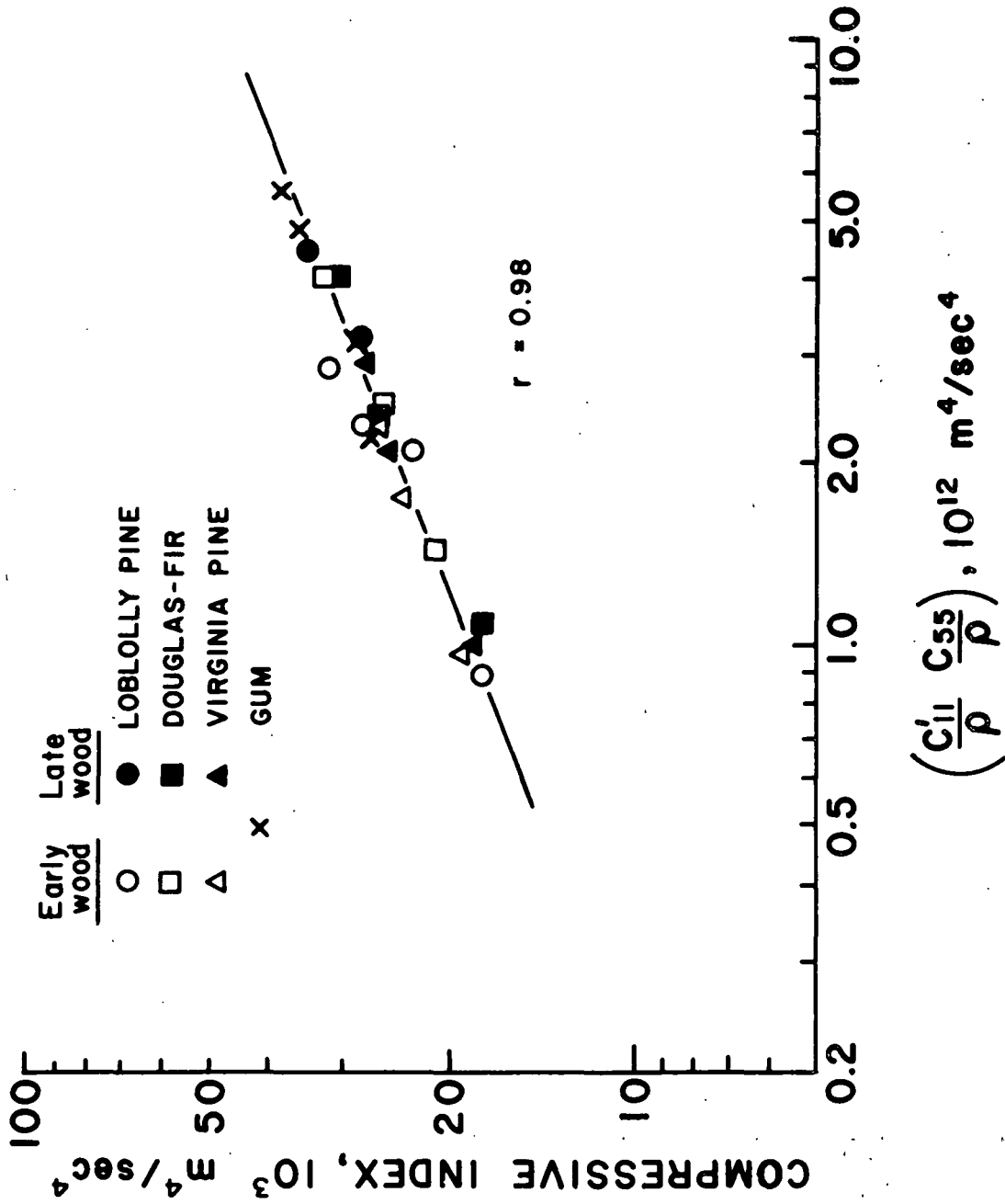


Fig. 4. The data in Fig. 2 plotted in terms of mass intensive parameters.

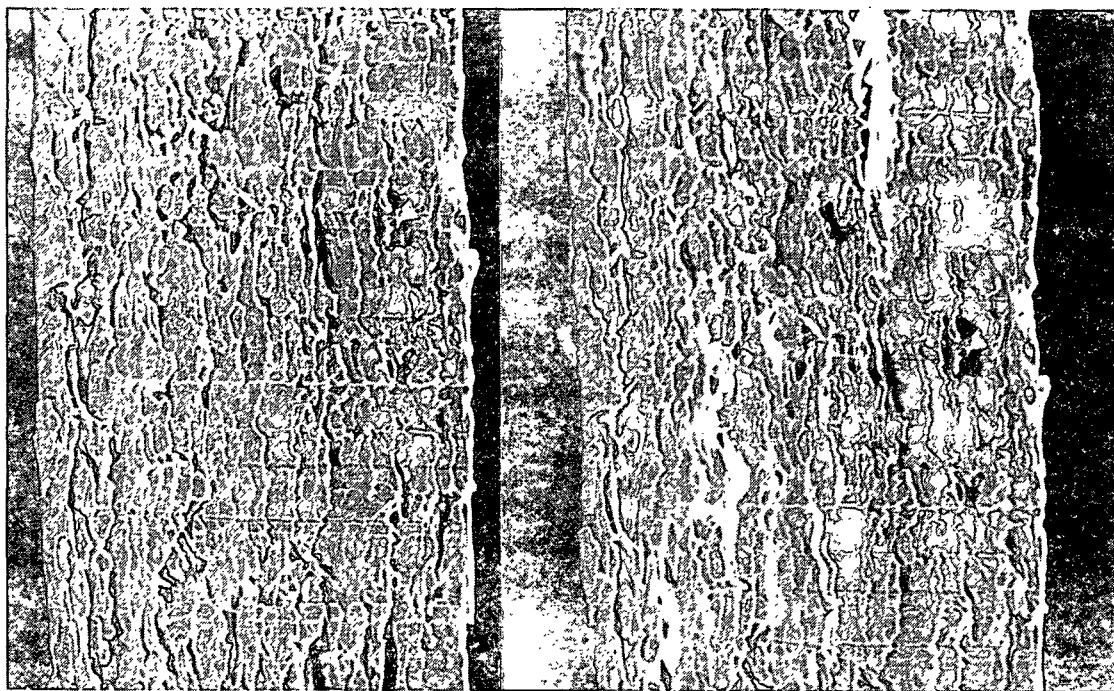


Fig. 1. S.E.M. micrographs of a linerboard sampler before and after edgewise compression. Common features can be compared if the compressed sample on the right is shifted upward. The white areas in the compressed sheet are caused by disruptions in a surface coating. The figure clearly shows sheet expansion and delamination between fiber layers in the compressed sheet.

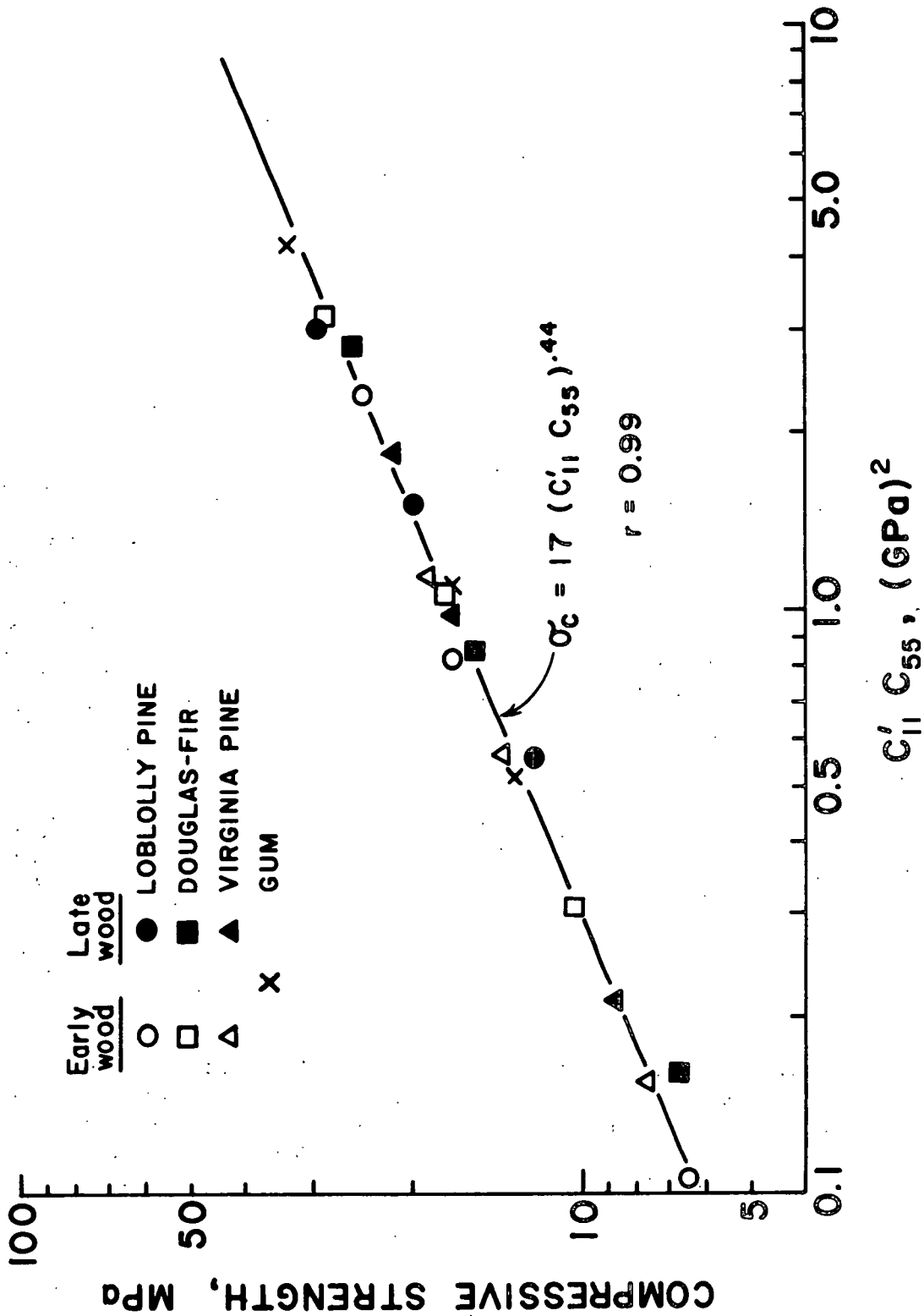


Fig. 2. Empirical relationship between compressive strength and in-plane stiffness times out-of-plane shear stiffness for handsheets of varying furnish and density.